

Dust dissipation timescales of protoplanetary disks and debris disks

HIROSHI MAESHIMA,^{1,2} TAKUYA KOJIMA,^{1,2} TAKAO NAKAGAWA,¹ JUNGMI KWON,¹ AND SATOSHI TAKITA¹

¹*Institute of Space and Astronautical Science, Japan Aerospace Exploration Agency, 3-1-1 Yoshinodai, Chuo, Sagami-hara, Kanagawa 252-5210, Japan*

²*Graduate School of Science, The University of Tokyo, Bunkyo-ku, 113-0033, Tokyo, Japan*

ABSTRACT

The far-infrared excess of stars with protoplanetary disks and debris disks is expected to provide us with key information on dust dissipation process in the outer disks. In order to reveal the typical behavior of the disks including objects fainter than the current survey limit, we stacked far-infrared images cut out from the image of *AKARI* all-sky survey in the 90 μm band (WIDE-S) on the basis of known object positions. We carried out two type of studies: one is the study on protoplanetary disks based on observations of T Tauri stars, and the other is the study on debris disks based on observations of A-type main sequence stars. Our studies show that, as disks evolve from protoplanetary disks to debris disks, the dust dissipation timescale becomes longer. This suggests that with disk evolution the dominant dust component changes from primordial dust, which remains small without growing into planetesimals, to secondary dust, which is formed by collisional destruction of planetesimals.

Keywords: Star-Formation: protoplanetary disks, circumstellar matter

1. INTRODUCTION

Protoplanetary disks (PPDs) are gaseous and dusty disks around pre-main sequence stars, and debris disks (DDs) are dusty disks around main sequence stars. Dust in the disks is warmed by stellar radiation and flux excess from photosphere flux is shown in the infrared wavelength region. As dust is farther from the central star, dust is colder and the peak of radiation becomes longer wavelength. Therefore, the far-infrared (FIR) excess of stars with the disks is expected to provide us with key information on dust dissipation process in the outer disks (~ 100 au). However, the number of objects detected in the FIR has been limited due to poor sensitivity of current observations. In order to reveal the typical behavior of PPDs and DDs including objects fainter than the current survey limit, we stacked FIR images cut out from the image of *AKARI* all-sky survey in the 90 μm band (WIDE-S) on the basis of known object positions.

We carried out two type of studies: one is on PPDs based on observations of K–M type T Tauri stars (TTSs), which are low mass pre-main sequence stars, and the other is on DDs based on observations of A-type main sequence stars.

2. DATA ANALYSIS & RESULTS

2.1. Protoplanetary disks

The first study is on PPDs based on observation K–M type TTSs. In order to make a unique catalog of TTSs closer than 200 pc, we collected multiple catalogs via *vizieR* catalog access tool. We collected 19 catalogs (Table 1), and there are 906 K–M type TTSs whose $H\alpha$ emission equivalent widths ($EW(H\alpha)$) are measured. The $H\alpha$ emission is caused by strong accretion onto TTSs, and becomes weaker with the evolution of a central star. Then we sorted these TTSs into 3 groups according to $EW(H\alpha)$ as an indicator of evolutionary stage: the TTSs whose $EW(H\alpha)$ is larger than 20 \AA are classified into a “high-EW” group, that between 10 \AA and 20 \AA into a “mid-EW” group, and that less than 10 \AA into a “low-EW” group. Next, according to several criteria, we exclude TTSs which are not suitable for stacking analysis. Finally, the high-EW group has 112 TTSs, the mid-EW group has 82 TTSs, and the low-EW group has 372 TTSs.

We stacked 90 μm IR images in each group, and aperture photometry was performed on the stacked images. The result is summarized in Table 2. We obtained 3 stacked images and their 90 μm fluxes respectively. The 90 μm IR fluxes decrease drastically in a typical TTS evolution timescale, and we conclude that decay timescale of the 90 μm IR flux of PPDs is 1–10 Myr. This timescale is roughly consistent with the dust dissipation timescales probed at near-IR and mid-IR wavelengths (Ribas et al. 2014).

Table 1. Selected 19 catalogs of TTSs

Cluster	Catalog
MBM12	Hearty et al. (2000)
ϵ Cha	Murphy et al. (2013)
ρ Oph	Wilking et al. (2005), Erickson et al. (2011)
R CrA	Neuhäuser et al. (2000)
Taurus-Auriga	McCabe et al. (2006), Slesnick et al. (2006b), Guieu et al. (2006), Rebull et al. (2010), Wichmann et al. (1996)
Upper Scorpius	Preibisch et al. (2001), Preibisch et al. (2002) Slesnick et al. (2006a), Slesnick et al. (2008)
LCC & UCL ^a	Mamajek et al. (2002)
MBM 55	Hearty et al. (1999)
Cha I	Frasca et al. (2015)
Lupus	Galli et al. (2015)
Cha II	Spezzi et al. (2008)

NOTE—(a) Lower Centaurus-Crux and Upper Centaurus-Lupus

Also, disk dust mass was estimated on the assumption of optically thin FIR emission and isothermal dust temperature ($T_{\text{dust}} = 20$ K). We estimate the dust masses as

$$M_{\text{dust}} \simeq \frac{F_{\nu, \text{dust}} d^2}{\kappa_{\nu} B_{\nu}(T_{\text{dust}})} = 10.6 M_{\oplus} \left(\frac{F_{\nu}}{1 \text{ Jy}} \right) \left(\frac{d}{150 \text{ pc}} \right)^2 \left(\frac{\kappa_{\nu}}{27.8 \text{ cm}^2 \text{ g}^{-1}} \right)^{-1} \left(\frac{B_{\nu}(T = 20 \text{ K})}{B_{\nu}(T_{\text{dust}})} \right)^{-1}, \quad (1)$$

where F_{ν} is the observed $90 \mu\text{m}$ flux, d is the distance ($d = 150$ pc), κ_{ν} is the dust opacity ($\kappa_{90\mu\text{m}} = 27.8 \text{ cm}^2 \text{ g}^{-1}$), and $B_{\nu}(T)$ is the flux of blackbody radiation.

Table 2. Result of stacking analysis on TTSs

Group	N_{stack}	EW(H α) [\AA]	observed flux [Jy]	disk dust mass [M_{\oplus}]
high-EW	112	67 ± 6	0.61 ± 0.03	6.5 ± 0.3
mid-EW	82	14.6 ± 0.3	0.086 ± 0.037	0.9 ± 0.4
low-EW	372	3.6 ± 0.1	0.041 ± 0.017	0.4 ± 0.2

2.2. Debris disks

The second study is on DDs based on observations of A-type main sequence stars. From Extended Hipparcos Compilation (Anderson & Francis 2012), 3,045 A-type main sequence stars were selected. In order to classify stars into 2 groups as the stellar age, the age estimation of stars was carried by two ways. First, if a star was judged to belong to a certain cluster from its position and velocity, we consider the stellar age is the same as the cluster age. Second, stellar ages, which cannot estimate by the first way, were determined by reference to Y^2 isochrones (Yi et al. 2003) in a H-R diagram. After the age estimation, the stars were sorted into two groups: the stars younger than 300 Myr is classified into ‘‘young A-star,’’ and older than 300 Myr into ‘‘old A-star.’’ Next, according to several criteria, we exclude stars which are not suitable for stacking analysis. Finally, young A-stars group has 1,214 stars and old A-star group has 1,501 stars.

We stacked $90 \mu\text{m}$ IR images in each group, and aperture photometry was performed on the stacked images (Figure 1). The result is summarized in Table 3. We obtained 2 stacked images (Figure 3) and $90 \mu\text{m}$ IR excess ratios (observed flux over expected photosphere flux). The expected photosphere flux in $90 \mu\text{m}$ is extrapolated from the K_s -band flux of the Two Micron All Sky Survey (2MASS) catalog (Cutri et al. 2003), assuming the spectra as that of the black body radiation. The $90 \mu\text{m}$ IR excess of young A-stars is significantly larger than that of old A-stars, and the $90 \mu\text{m}$ IR excess become fainter as central stars become older. The result is consistent with the previous result (Su et al. 2006). By applying steady-state model (Wyatt et al. 2007), we suggest that the $90 \mu\text{m}$ IR excess ratios of A-stars decreases in 230_{-100}^{+160} Myr (Figure 4).

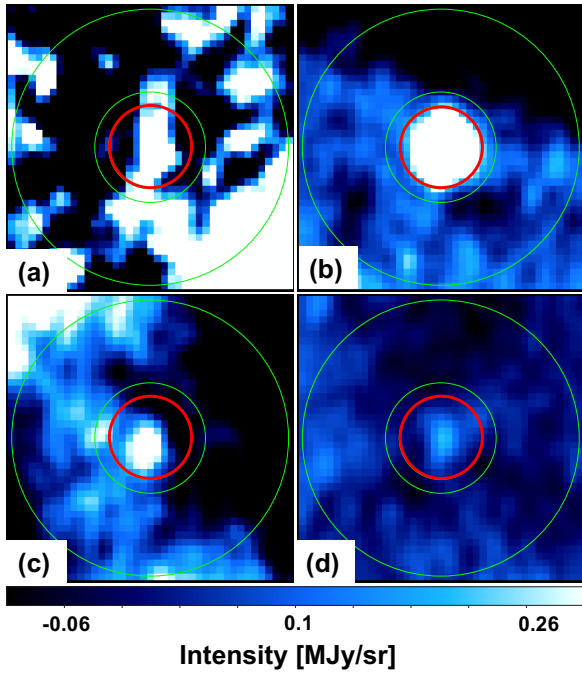


Figure 1. (a) An example of single TTS image. (b) The stacked image of 112 high-EW TTSs. (c) The stacked image of 82 mid-EW TTSs. (d) The stacked image of 372 low-EW TTSs. The red circles show the aperture and the region enclosed by two green circles show sky annulus. The field of view is $10'15'' \times 10'15''$

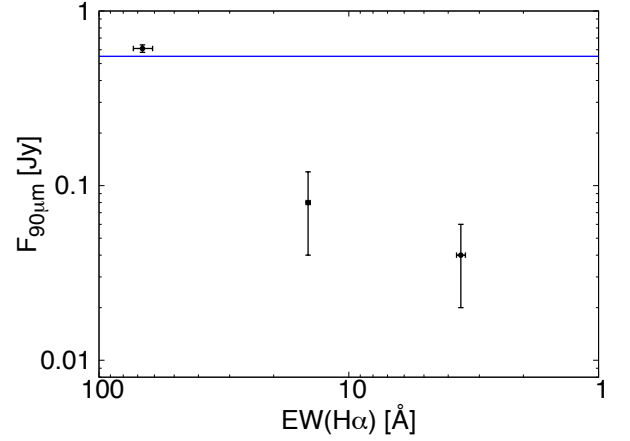


Figure 2. Observed fluxes of stacked TTSs as a function of mean $EW(H\alpha)$. The black symbols mark this work. The blue line shows 5σ detection limit of a single point source in WIDE-S All-Sky Survey mode.

Table 3. Results of stacking analysis on A-type main sequence stars

group	N_{stack}	age [Myr]	observed flux [Jy]	$90 \mu\text{m}$ IR excess ratio
young A-stars	1,214	97 ± 78	0.041 ± 0.005	12.3 ± 1.5
old A-stars	1,501	570 ± 197	0.029 ± 0.004	5.61 ± 0.88

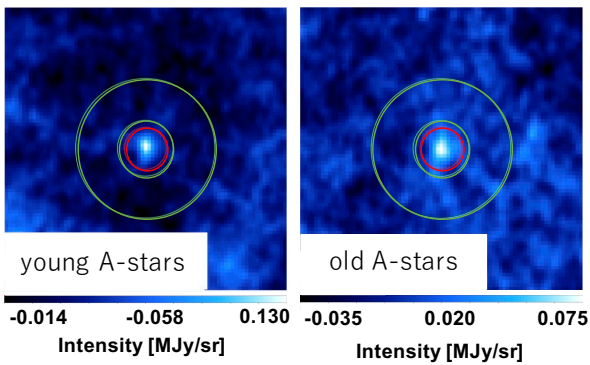


Figure 3. Left panel: The stacked image of 1,214 young A-stars. Right Panel: The stacked image of 1,501 old A-stars. The red circle indicates the same as Figure 1. The field of view is $20' \times 20'$

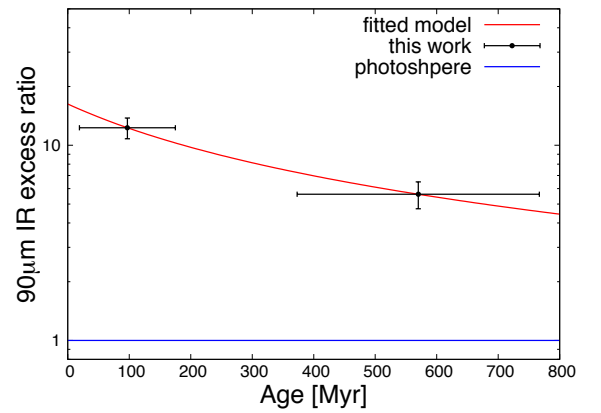


Figure 4. The $90 \mu\text{m}$ IR excess ratios of stacked A-stars as a function of mean age. The green line shows the fitted theoretical model line.

3. DISCUSSION

We conclude that the decay time of 90 μm flux of PPDs is 1–10 Myr. This timescale is consistent with “primordial dust” dissipation timescale. Primordial dust remains small without growing into planetesimals and dissipate in a few Myr by radiation pressure and by Poynting-Robertson effect (Williams et al. 2011). We suggest that the decay time of 90 μm IR excess ratio of DDs is about 230 Myr. This timescale is consistent with “secondary dust” dissipation timescale. Secondary dust is formed by collisional destruction of planetesimals. Because of dust provision by the destruction, effective dissipation timescale of secondary dust is extended by ~ 100 Myr. Our results show that as disks evolve from PPDs to DDs, dust dissipation timescale becomes about ten times longer. This suggests that with disk evolution the dominant dust component changes from primordial dust to secondary dust.

ACKNOWLEDGMENTS

This research is based on observations with *AKARI*, a JAXA project with the participation of ESA. We thank Mr. Yasuhiro Matsuki for the original code of the stacking analysis which is the basis of our studies. This research has made use of the VizieR catalogue access tool, CDS, Strasbourg, France.

REFERENCES

- Anderson, E., & Francis, C. 2012, *Astronomy Letters*, 38, 331
- Cutri, R. M., Skrutskie, M. F., van Dyk, S., et al. 2003, *The IRSA 2MASS All-Sky Point Source Catalog*.
- Erickson, K. L., Wilking, B. A., Meyer, M. R., Robinson, J. G., & Stephenson, L. N. 2011, *AJ*, 142, 140
- Frasca, A., Biazzo, K., Lanzafame, A. C., et al. 2015, *A&A*, 575, A4
- Galli, P. A. B., Bertout, C., Teixeira, R., & Ducourant, C. 2015, *A&A*, 580, A26
- Guieu, S., Dougados, C., Monin, J.-L., Magnier, E., & Martín, E. L. 2006, *A&A*, 446, 485
- Hearty, T., Magnani, L., Caillault, J.-P., et al. 1999, *A&A*, 341, 163
- Hearty, T., Fernández, M., Alcalá, J. M., Covino, E., & Neuhäuser, R. 2000, *A&A*, 357, 681
- Mamajek, E. E., Meyer, M. R., & Liebert, J. 2002, *AJ*, 124, 1670
- McCabe, C., Ghez, A. M., Prato, L., et al. 2006, *ApJ*, 636, 932
- Murphy, S. J., Lawson, W. A., & Bessell, M. S. 2013, *MNRAS*, 435, 1325
- Neuhäuser, R., Walter, F. M., Covino, E., et al. 2000, *A&AS*, 146, 323
- Preibisch, T., Guenther, E., & Zinnecker, H. 2001, *AJ*, 121, 1040
- Preibisch, T., Brown, A. G. A., Bridges, T., Guenther, E., & Zinnecker, H. 2002, *AJ*, 124, 404
- Rebull, L. M., Padgett, D. L., McCabe, C.-E., et al. 2010, *ApJS*, 186, 259
- Ribas, Á., Merín, B., Bouy, H., & Maud, L. T. 2014, *A&A*, 561, A54
- Slesnick, C. L., Carpenter, J. M., & Hillenbrand, L. A. 2006a, *AJ*, 131, 3016
- Slesnick, C. L., Carpenter, J. M., Hillenbrand, L. A., & Mamajek, E. E. 2006b, *AJ*, 132, 2665
- Slesnick, C. L., Hillenbrand, L. A., & Carpenter, J. M. 2008, *ApJ*, 688, 377-397
- Spezzi, L., Alcalá, J. M., Covino, E., et al. 2008, *ApJ*, 680, 1295-1318
- Su, K. Y. L., Rieke, G. H., Stansberry, J. A., et al. 2006, *ApJ*, 653, 675
- Wichmann, R., Krautter, J., Schmitt, J. H. M. M., et al. 1996, *A&A*, 312, 439
- Wilking, B. A., Meyer, M. R., Robinson, J. G., & Greene, T. P. 2005, *AJ*, 130, 1733
- Williams, J. P., & Cieza, L. A. 2011, *ARA&A*, 49, 67
- Wyatt, M. C., Smith, R., Su, K. Y. L., et al. 2007, *ApJ*, 663, 365
- Yi, S. K., Kim, Y.-C., & Demarque, P. 2003, *ApJS*, 144, 259